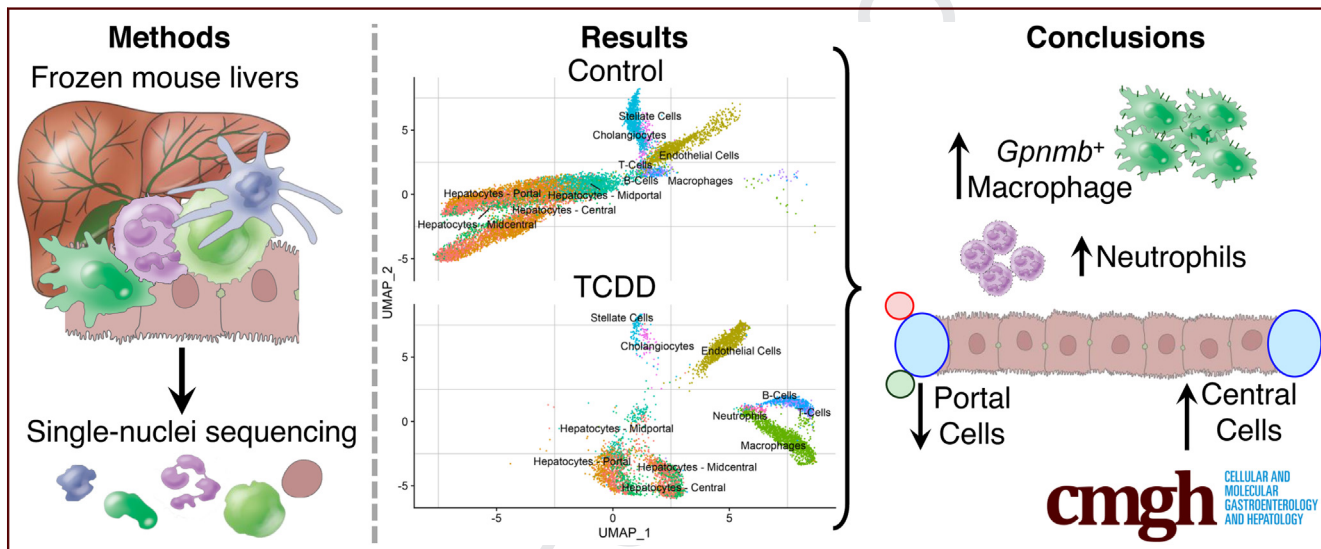


ORIGINAL RESEARCH

Single-Nuclei RNA Sequencing Assessment of the Hepatic Effects of 2,3,7,8-Tetrachlorodibenzo-*p*-dioxinRance Nault,^{1,2} Kelly A. Fader,^{1,2} Sudin Bhattacharya,^{1,3,4} and Tim R. Zacharewski^{1,2}

¹Institute for Integrative Toxicology, Michigan State University, East Lansing, Michigan; ²Department of Biochemistry and Molecular Biology, Michigan State University, East Lansing, Michigan; ³Department of Biomedical Engineering, Institute for Quantitative Health Science and Engineering, Michigan State University, East Lansing, Michigan; and ⁴Department of Pharmacology and Toxicology, Michigan State University, East Lansing, Michigan



SUMMARY

The application of single-nuclei RNA sequencing is demonstrated for the evaluation of a hepatotoxicant highlighting key considerations in study design. The potent aryl hydrocarbon receptor agonist 2,3,7,8-tetrachlorodibenzo-*p*-dioxin is shown to elicit cell-specific responses and alter relative population sizes.

BACKGROUND AND AIMS: Characterization of cell specific transcriptional responses to hepatotoxicants is lost in the averages of bulk RNA-sequencing (RNA-seq). Single-cell/nuclei RNA-seq technologies enable the transcriptomes of individual cell (sub)types to be assessed within the context of *in vivo* models.

METHODS: Single-nuclei RNA-sequencing (snSeq) of frozen liver samples from male C57BL/6 mice gavaged with sesame oil vehicle or 30 µg/kg 2,3,7,8-tetrachlorodibenzo-*p*-dioxin (TCDD) every 4 days for 28 days was used to demonstrate the application of snSeq for the evaluation of xenobiotics.

RESULTS: A total of 19,907 genes were detected across 16,015 nuclei from control and TCDD-treated livers. Eleven cell (sub)types reflected the expected cell diversity of the liver including distinct pericentral,

midzonal, and periportal hepatocyte subpopulations. TCDD altered relative proportions of cell types and elicited cell-specific gene expression profiles. For example, macrophages increased from 0.5% to 24.7%, while neutrophils were only present in treated samples, consistent with histological evaluation. The number of differentially expressed genes (DEGs) in each cell type ranged from 122 (cholangiocytes) to 7625 (midcentral hepatocytes), and loosely correlated with the basal expression level of *Ahr*, the canonical mediator of TCDD and related compounds. In addition to the expected functions within each cell (sub)types, RAS signaling and related pathways were specifically enriched in nonparenchymal cells while metabolic process enrichment occurred primarily in hepatocytes. snSeq also identified the expansion of a Kupffer cell subtype highly expressing *Gpnmb*, as reported in a dietary NASH model.

CONCLUSIONS: We show that snSeq of frozen liver samples can be used to assess cell-specific transcriptional changes and population shifts in models of hepatotoxicity when examining freshly isolated cells is not feasible. (*Cell Mol Gastroenterol Hepatol* 2020;■:■-■; <https://doi.org/10.1016/j.jcmgh.2020.07.012>)

Keywords: Transcriptomics; TCDD; Hepatotoxicant; Cellular Heterogeneity.

117
 118 **T**he liver is particularly susceptible to toxicity due to its
 119 close association with the gastrointestinal tract and
 120 xenobiotic metabolism capacity.¹ Liver toxicity is the pri-
 121 mary driver of drug candidate attrition and a common cause
 122 of market withdrawal.² Similarly, environmental contam-
 123 inant exposure is implicated in liver damage in humans,
 124 evidenced by increased levels of the liver damage biomarker
 125 alanine aminotransferase in epidemiological studies.^{3–5}
 126 Moreover, environmental contaminants such as 2,3,7,8-
 127 tetrachlorodibenzo-*p*-dioxin (TCDD) are potential contrib-
 128 uting factors in the etiology of complex metabolic diseases
 129 such as obesity, type II diabetes, and nonalcoholic fatty liver
 130 disease.^{3–5} For example, aryl hydrocarbon receptor (AhR)
 131 agonists such as TCDD and related compounds promote
 132 hepatic lipid accumulation (steatosis) and its progression to
 133 steatohepatitis (NASH) with fibrosis in mice,^{6–8} while
 134 epidemiological studies suggest an association with meta-
 135 bolic disease in humans.^{9,10}

136 Although bulk “omic” strategies have uncovered impor-
 137 tant knowledge on the mechanisms of hepatotoxins, key
 138 molecular events, as well as the significance of temporal,
 139 spatial, and cellular heterogeneity, remain poorly under-
 140 stood within the *in vivo* context of a tissue.¹¹ Single-cell
 141 transcriptomic technologies provide the opportunity to
 142 investigate the transcriptomic responses to exogenous
 143 agents while also considering cellular heterogeneity and
 144 putative cell-cell interactions.¹² Single-cell RNA sequencing
 145 (scSeq) can query the transcriptome at unprecedented
 146 resolution, characterizing rare cell types and developmental
 147 processes,^{13,14} and further elucidate the significance of tis-
 148 sue spatial organization.^{15,16} scSeq analysis of a diet-
 149 induced NASH model revealed the expansion of a novel
 150 Kupffer cell (KC) subtype termed NASH-associated macro-
 151 phages (NAMs), as well as altered vascular signaling.¹⁷ It is
 152 also established that drugs and toxicants elicit spatial
 153 (zonal) toxicities as in the case of acetaminophen, which
 154 primarily affects the centrilobular region due to higher
 155 expression levels of xenobiotic metabolizing enzymes.¹⁸
 156 Conversely, TCDD elicits periportal hepatotoxicity despite
 157 preferential accumulation in the centrilobular region due to
 158 sequestration by induced CYP1A2 levels.^{19,20} It remains
 159 unclear how transcriptional networks are implicated in
 160 these zonal toxicities. Single-cell analysis is expected to
 161 further elucidate the role of specific cell (sub)populations in
 162 toxicity and models of liver disease progression.

163 Preclinical drug or chemical toxicity assessments typi-
 164 cally involve dose-response designs that present numerous
 165 challenges for implementing scSeq, primarily the required
 166 use of freshly isolated cells. Ongoing efforts to minimize
 167 experimental animal use also demand that studies maximize
 168 the extraction of relevant data including gross pathology,
 169 clinical chemistry, and histopathology. The impact of diurnal
 170 rhythm in large studies places additional logistic constraints
 171 regarding sample collection within a specific time win-
 172 dow.²¹ Most importantly, it is difficult to predict how
 173 treatment and/or disease pathologies impact cell pop-
 174 ulations, structure and viability, digestion efficacy, and cell
 175 type selection for single-cell analysis without extensive *a* priori validation. Nuclei-based approaches address many of

176 these challenges and produce results comparable to single-
 177 cell approaches.^{14,22–24} Notably, single-nuclei RNA sequencing
 178 (snSeq) can be performed on frozen samples, providing the
 179 best solution for traditional toxicology assessments. In the
 180 presented study, snSeq was used to evaluate the hepatic ef-
 181 fects of TCDD. snSeq analysis using frozen liver samples
 182 showed TCDD-elicted cell population shifts and cell-specific
 183 differential gene expression consistent with the progression
 184 of hepatic steatosis to NASH with fibrosis.

Results

snSeq Identifies Major Liver Cell (Sub)types in Vehicle and TCDD-Treated Mice

We adapted a scSeq protocol for frozen cancer tissue biopsy samples that was compatible with the 10x Genomics (Pleasanton, CA) technology to characterize gene expression in nuclei isolated from mouse liver samples treated with either sesame oil vehicle or 30 µg/kg TCDD. A total of 16,015 individual nuclei transcriptomes (9981 and 6034 in vehicle and TCDD-treated, respectively) were characterized across 2 biological replicates per treatment group after quality control and doublet removal. The average number of expressed genes detected in each sample was 17,920, consistent with our published bulk RNA sequencing (RNA-seq) assessments collected using a similar study design.^{6,25} The median number of unique detected genes in individual nuclei was 1694, with a median unique molecular identifier (transcript) count of 3385 per nuclei. As expected with a nuclear preparation, there was negligible expression of mitochondrial genes, and long noncoding RNAs (lncRNAs) such as *Malat1* and *Gm42416* were the most abundantly expressed genes.^{23,24} The number of unique expressed genes and median unique molecular identifier count (1500 and 3805, respectively), as well as total expressed genes (19,907), was similar to a published 10x Genomics liver single-cell dataset (19,349),¹⁶ lending further confidence in our snSeq approach. Cell Ranger (10x Genomics) detected some ambient RNA contamination in some samples, likely owing to the lysis of cells during nuclei isolation.²⁶ However, neither of the common indicators of ambient RNA contamination (mitochondrial or hemoglobin gene expression—*Mt* or *Hba/Hbb*, respectively) were elevated in our samples (<https://doi.org/10.6084/m9.figshare.12728411>). Consequently, ambient RNA decontamination tools were not used.

Integration and clustering of nuclei transcriptomic profiles identified 11 clusters, of which only the neutrophil cluster was unique to TCDD treatment (Figure 1A and D).

Abbreviations used in this paper: AhR, aryl hydrocarbon receptor; DEG, differentially expressed gene; GEO, Gene Expression Omnibus; GSKB, Gene Set Knowledgebase; KC, Kupffer cell; lncRNA, long noncoding RNA; mRNA, messenger RNA; NAM, nonalcoholic steatohepatitis-associated macrophage; NASH, nonalcoholic steatohepatitis; NPC, nonparenchymal cell; PND, postnatal day; RNA-seq, RNA sequencing; scSeq, single-cell RNA sequencing; snSeq, single-nuclei RNA sequencing; TCDD, 2,3,7,8-tetrachlorodibenzo-*p*-dioxin.

© 2020 The Authors. Published by Elsevier Inc. on behalf of the AGA Institute. This is an open access article under the CC BY-NC-ND license (<http://creativecommons.org/licenses/by-nc-nd/4.0/>).

2352-345X

<https://doi.org/10.1016/j.jcmgh.2020.07.012>

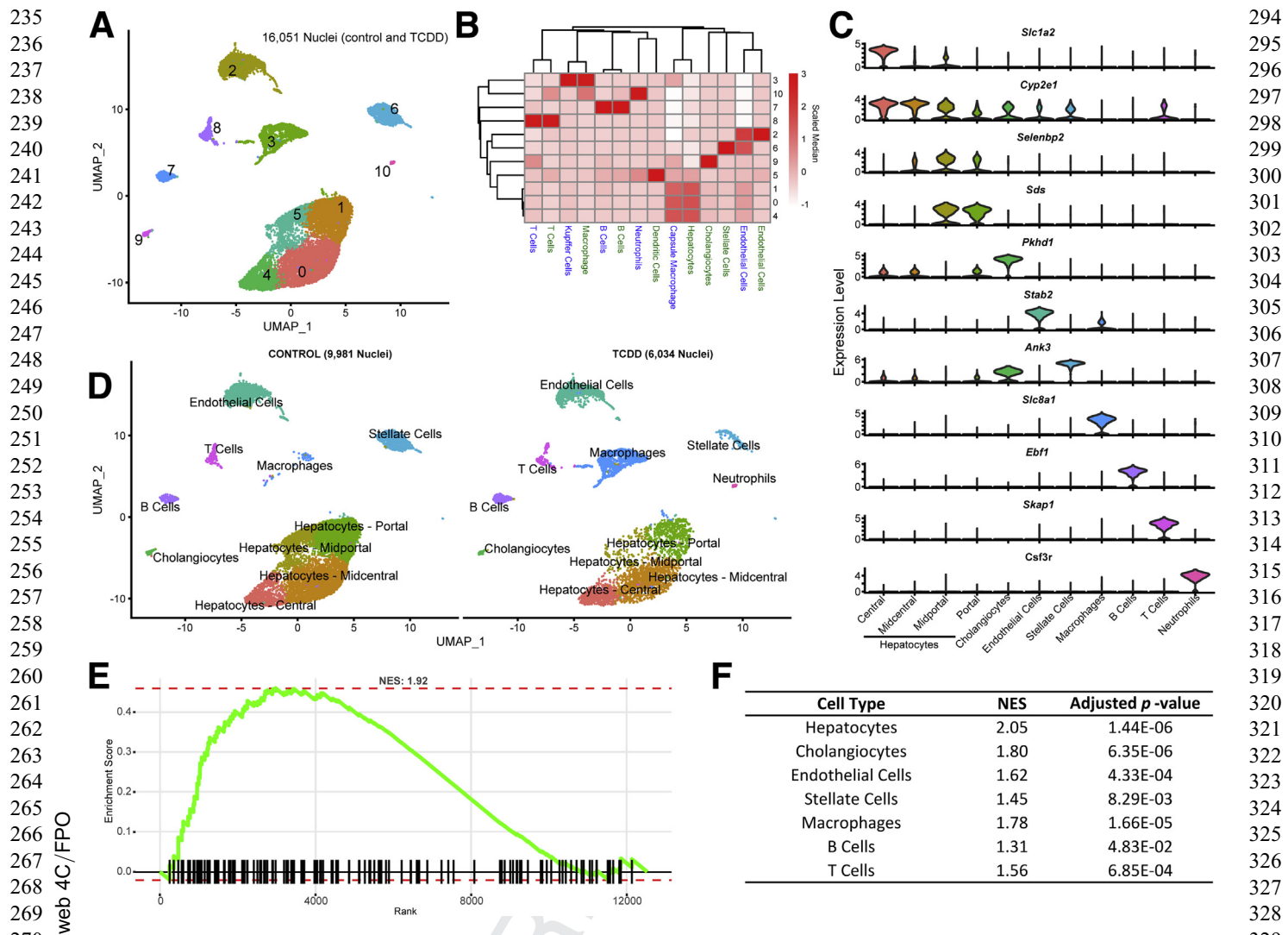


Figure 1. snSeq analysis of nuclei isolated from frozen liver samples of mice gavaged every 4 days for 28 days with sesame oil vehicle or 30 µg/kg TCDD. (A) UMAP visualization of nuclei isolated from vehicle and TCDD-treated liver samples clustered based on gene expression profile similarity. (B) Label transfer prediction from published liver scSeq data—Bahr Halpern et al¹⁴ in blue, Xiong et al¹⁶ in green—was used to identify similar clusters for annotation. (C) Expression distribution for distinguishing (largest average fold-change, adjusted $P \leq .05$) marker genes within each specific cell type. Color of clusters in panel C correspond to cell type clusters in panel A. (D) UMAP visualization of annotated nuclei in control and TCDD-treated samples. Gene set enrichment analysis of nuclear biased genes (first quartile)³¹ using genes ranked from most to least abundantly expressed in our nuclei dataset compared with Xiong et al's¹⁶ whole-cell data was performed for (E) all cell types and (F) paired cell types identified in both datasets. NES, normalized enrichment score.

Nuclei clusters were initially annotated by integrating our dataset with 2 published scSeq datasets and comparing annotation assignments (Figure 1B).^{15,17} Initial annotations were subsequently corroborated using the expression of known markers for specific cell types based on published reports or panglaoDB.²⁷ For example, nuclei with higher levels of Stabilin 2 (*Stab2*) (Figure 1B and C), an expression marker for hepatic sinusoidal endothelial cells,²⁸ were identified as “Endothelial Cell” nuclei in our dataset, as reported by Xiong et al¹⁶ in a diet-induced NASH model. Similarly, cholangiocyte expression profiles aligned with a distinct nuclei cluster (Figure 1B).¹⁶ Although the classical cholangiocyte marker, SRY-Box 9 (*Sox9*), was not expressed in our nuclei, the similarity between the expression profiles

in our dataset and cells expressing *Sox9* reported by Xiong et al¹⁶ suggested that these nuclei are indeed cholangiocytes. Examination of distinguishing markers for each nuclei cluster (Figure 1C) identified *Pkh1d* (also known as fibrocystin) as one of the distinguishing markers for cholangiocytes.²⁹ Other distinguishing markers such as *Ebf1*, important in B cell development,³⁰ and the T cell adaptor *Skap1*,³¹ were also in agreement with cluster annotations.

Our dataset suggests that *Sox9* may be less abundant in nuclei sample preparations, consistent with previous reports indicating some genes exhibit nuclear or cytosolic biases.^{23,24,32} Comparison of our dataset with Xiong et al¹⁶ using a similar model and the same technology shows

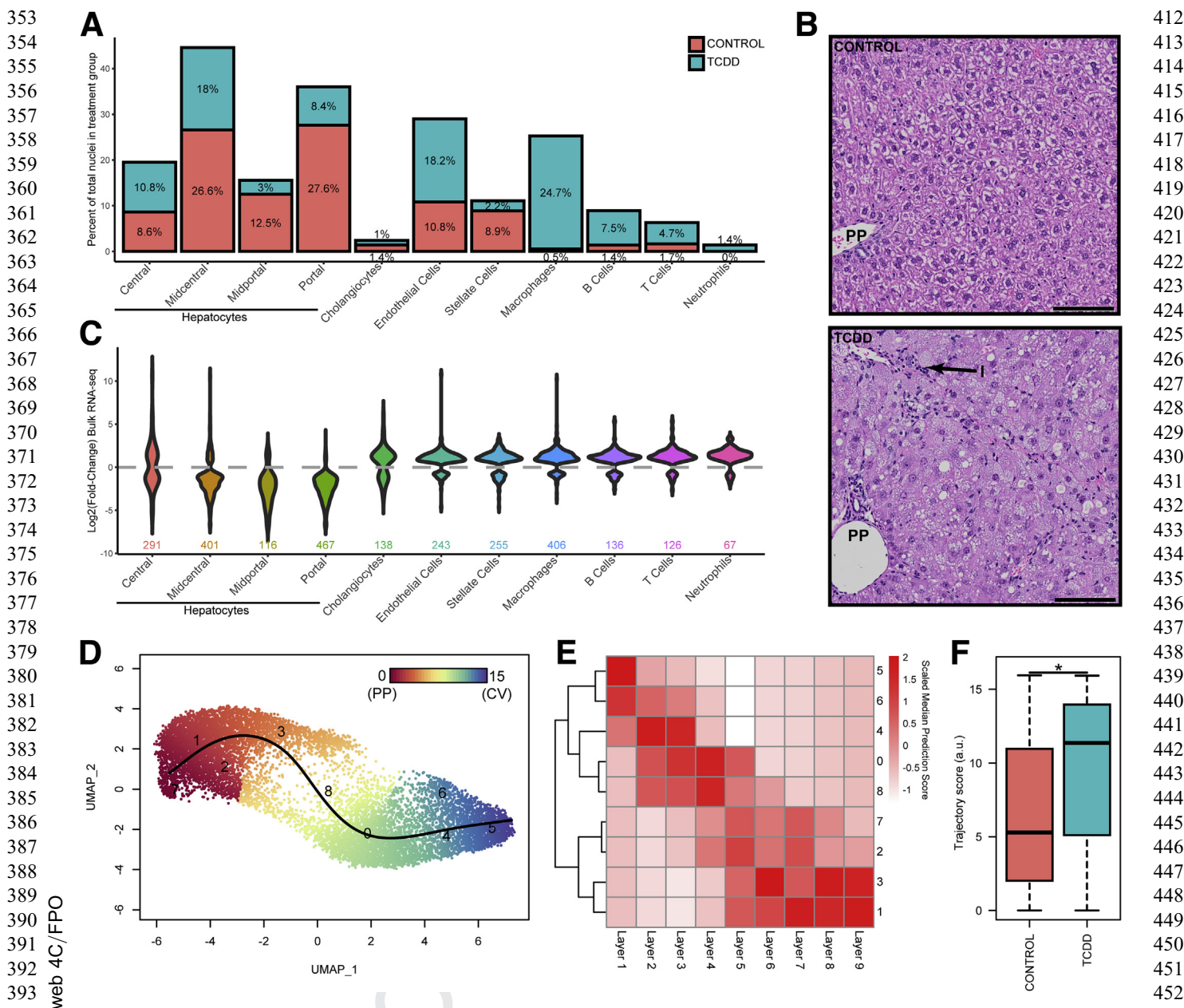


Figure 2. Hepatic cell population shifts in response to TCDD. (A) Percentage of nuclei represented in cell type-specific clusters in control and treated samples. (B) Representative liver photomicrographs from control and TCDD-treated samples using the same study design³² showing peripoortal (PP) immune cell infiltration (I). Scale bar = 100 μ m. (C) Violin plots of fold-change expression distribution for genes defining cell type clusters (adjusted $P \leq .05$) in TCDD-elicited bulk RNA-seq dataset. (D) Reclustering and trajectory analysis of only hepatocyte nuclei from vehicle control and TCDD treatment groups using a resolution of 1.2 to identify 9 clusters in order to (E) compare snSeq gene expression with the 9 distinct spatially resolved hepatocyte layers defined Halpern et al.¹⁵ (F) Nuclei distribution along the trajectory determined in control and TCDD-treated samples. The asterisk indicates a significant difference in distribution with TCDD causing a shift in the hepatocyte nuclei population toward the central cluster/layer as determined by the Kolmogorov-Smirnov test ($P \leq .05$).

excellent concordance in identifying genes expressed in liver cells (16,789; 84%–87%) despite Xiong et al's enrichment for nonparenchymal cells. However, it is evident that relative levels of certain genes differ, particularly lncRNA's. Comparisons of nuclear and cytoplasmic gene expression in liver cells (mixed cell types) identified *Mlxip1* (ChREBP) and *Nrlp6* as retained nuclear genes, as well as the lncRNA *Neat1*.³² In agreement, our dataset

exhibited greater expression of these genes compared with whole-cell liver expression data Xiong et al (<https://doi.org/10.6084/m9.figshare.12728441>)¹⁶ We performed gene set enrichment analysis on ranked genes from nuclear-biased (elevated fold change in our vehicle control dataset compared with control whole cell data) to cytosolic/whole cell-biased (elevated in control single-cell data compared with our vehicle control dataset) using nuclear

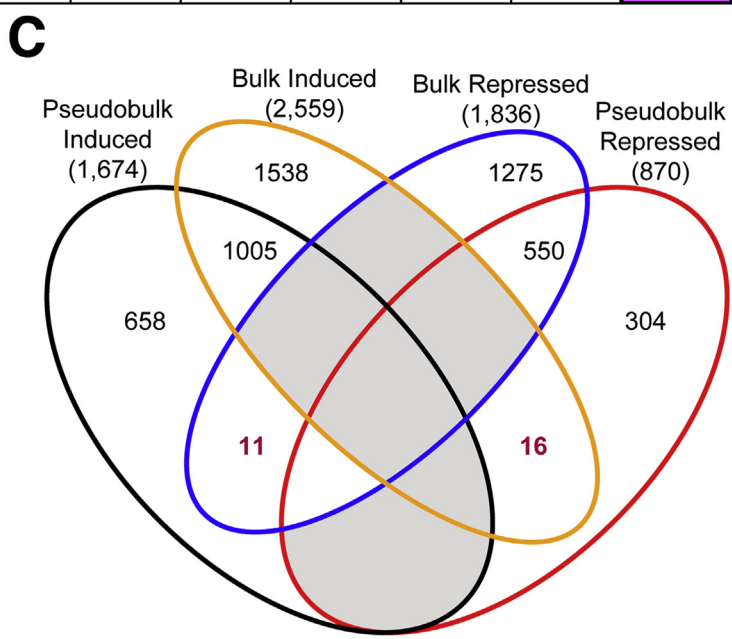
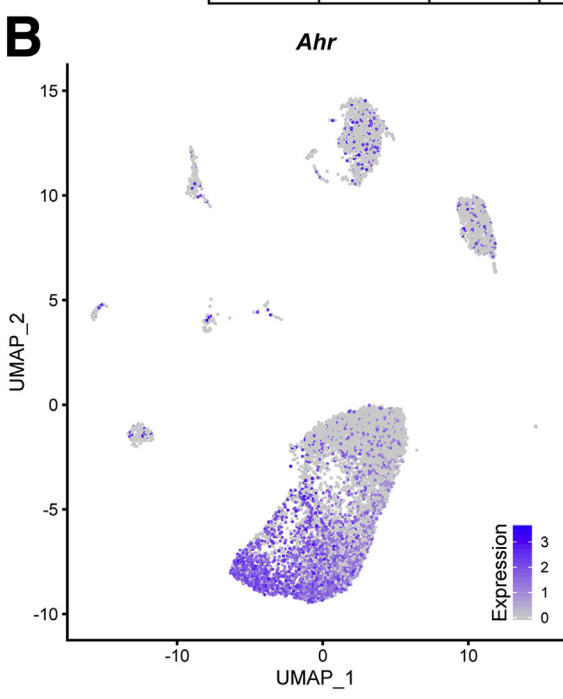
471 biased genes (top first percentile) identified by Bahar
 472 **Q6** Halpern et al³¹ as the gene set. Figure 1E and F shows our
 473 single-nuclei gene expression dataset is indeed enriched in
 474 nuclear biased genes in all cell types.

TCDD Shifted Cell Type Proportions

530 TCDD elicited shifts in the relative proportions of nuclei
 531 clusters (Figure 2A). Macrophages increased from 0.5% in
 532 control samples to 24.7% in TCDD-treated samples,
 533

A

		Hepatocytes				Cholangiocytes									
		Central	Midcentral	Midportal	Portal	Endothelial Cells		Stellate Cells		Macrophages		B-Cells		T-Cells	
Hepatocytes	Central	7529	6120	1182	4955	88	2131	481	206	365	411				
	Midcentral	81.3 - 80.3%	7625	1250	5302	87	1971	496	235	380	404				
Hepatocytes	Midportal	15.7 - 83.9%	16.4 - 88.7%	1409	1305	70	585	226	148	220	206				
	Portal	65.8 - 78.1%	69.5 - 83.5%	92.6 - 20.6%	6346	82	1646	455	198	324	347				
Cholangiocytes	Cholangiocytes	1.2 - 72.1%	1.1 - 71.3%	5 - 57.4%	1.3 - 67.2%	122	80	55	38	48	55				
	Endothelial Cells	28.3 - 66.3%	25.8 - 61.3%	41.5 - 18.2%	25.9 - 51.2%	65.6 - 2.5%	3216	443	220	401	463				
Hepatocytes	Stellate Cells	6.4 - 54.1%	6.5 - 55.8%	16 - 25.4%	7.2 - 51.2%	45.1 - 6.2%	13.8 - 49.8%	889	127	149	166				
	Macrophages	2.7 - 64%	3.1 - 73%	10.5 - 46%	3.1 - 61.5%	31.1 - 11.8%	6.8 - 68.3%	14.3 - 39.4%	322	134	141				
Hepatocytes	B Cells	4.8 - 66.1%	5 - 68.8%	15.6 - 39.9%	5.1 - 58.7%	39.3 - 8.7%	12.5 - 72.6%	16.8 - 27%	41.6 - 24.3%	552	301				
	T Cells	5.5 - 63%	5.3 - 62%	14.6 - 31.6%	5.5 - 53.2%	45.1 - 8.4%	14.4 - 71%	18.7 - 25.5%	43.8 - 21.6%	54.5	652				



589 accompanied by other immune cells such as B cells (1.4% to
 590 7.5%), T cells (1.7% to 4.7%), and neutrophils (0.0% to
 591 1.4%). This is consistent with TCDD-induced inflammation
 592 (Figure 2B) and elevated levels of proinflammatory cyto-
 593 kines, including tumor necrosis factor- α and interleukin-6.⁷
 594 Overall, the relative proportion of hepatocytes in TCDD-
 595 treated samples was reduced by 46.6% (75.3% in control
 596 samples compared with 40.2% in treated samples). All
 597 zones were reduced, except for central hepatocytes, which
 598 increased from 8.6% to 10.8% (Figure 2A). Note that dis-
 599 tinguishing between decreases in relative proportion of cell
 600 types reflecting cell death, loss of cell types during pro-
 601 cessing, or a true shift in relative levels is challenging.
 602 Previous studies using the same study design did not report
 603 cell death from histological evaluation.³³ These challenges
 604 are further explored in the subsequent discussion.

605 To further investigate cell population shifts, we re-
 606 examined our published hepatic bulk RNA-seq (same spe-
 607 cies, strain, sex, age, treatment regimen, dose, and duration
 608 of exposure)⁶ for TCDD-elicited fold-change distribution of
 609 genes identified as cell type markers (adjusted $P \leq .05$)
 610 (Figure 2C). Overall, marker gene expression for midcentral,
 611 midportal, and portal hepatocytes was repressed in our bulk
 612 RNA-seq dataset, as evidenced by the bulk RNA-seq \log_2 (-
 613 fold-change) distribution ≤ 0 (wider below the gray line).
 614 Conversely, marker genes for cholangiocytes, endothelial
 615 cells, stellate cells, and immune cells were induced.
 616 Comparing the changes in relative proportions (Figure 2A)
 617 to differential gene expression in bulk RNA-seq (Figure 2C)
 618 confirms the impact of TCDD on cell population shifts in
 619 bulk RNA-seq analysis. Specifically, central hepatocyte
 620 marker genes were repressed despite a modest increase in
 621 relative cell numbers suggesting TCDD effects on gene
 622 expression. In contrast, macrophage marker induction con-
 623 comitant with increased macrophage number makes it
 624 difficult to distinguish a direct effect on gene expression
 625 from an increase in the number of infiltrating cells with
 626 basal gene expression. The limited ability to delineate these
 627 effects using bulk RNA-seq demonstrates another advantage
 628 of a single-cell/nuclei analysis.

630 Characterization of Spatially Resolved 631 Hepatocytes

632 To investigate zonal gene expression using snSeq data,
 633 hepatocyte nuclei from both treatment groups were
 634 selected, reintegrated, and reclustered to obtain 9 clusters,
 635 guided by the 9 hepatocyte zones (ie, layers) defined by
 636 Bahar Halpern et al (Figure 2D).¹⁶ Our hepatocyte nuclei
 637

638 clusters demonstrate high similarity to the transcriptomes
 639 of the different cell layers defined by Bahar Halpern et al
 640 (Figure 2E).¹⁶ Specifically, the nuclei cluster labeled 5 was
 641 most similar to layer 1 cells, while clusters 1 and 3 were
 642 most like layers 8 and 9. Zonal trajectory assessed using
 643 Slingshot³⁴ shows a transition in gene expression profiles
 644 from cluster 5 to 1, reflecting a gradient from central (layer
 645 1) to portal (layer 9) (Figure 2D and E). Cluster 7 was less
 646 defined, though closer examination identified the expression
 647 of portal markers, along with elevated expression of met-
 648 allothioneins (*Mt1* and *Mt2*) equally expressed in control
 649 and treated samples (<https://doi.org/10.6084/m9.figshare.12728507>). Comparing zonal distribution between control
 650 and treated nuclei revealed a shift toward central hepato-
 651 cyte expression, suggesting that TCDD caused a loss of
 652 portal hepatocyte gene expression, or possibly a loss of
 653 portal hepatocytes during sample preparation (Figure 2F).
 654 TCDD elicits periportal hepatotoxicity, and therefore the
 655 loss of identity from de- or transdifferentiation cannot be
 656 distinguished from cell-specific cytotoxicity.

657 Differential Gene Expression Elicited by TCDD Is 658 Largely Cell Type Specific

659 Of the 19,907 genes detected across all liver cell types,
 660 10,951 were identified as differentially expressed, compara-
 661 ble to the 9313 (of 19,935) DEGs reported in our com-
 662 parable bulk RNA-seq study.⁶ Hepatocyte subtypes
 663 exhibited the greatest similarity in differential gene
 664 expression with 92.6% ($n = 1305$ of 1409) of midportal
 665 DEGs overlapping with portal DEGs (Figure 3A). However,
 666 this only represents 20.6% ($n = 1306$ of 6346) of portal
 667 DEGs, suggesting that midportal cells may be a subset of
 668 portal hepatocytes. Cholangiocytes compared with macro-
 669 phages shared the fewest overlapping DEGs, with only 38 in
 670 common (31.1% and 11.8% of DEGs, respectively). Only 28
 671 genes were differentially expressed in all cell types, with 26
 672 repressed in every cell type. Only cadherin 18 (*Cdh18*) was
 673 induced in all cells, while dihydropyrimidine dehydrogenase
 674 (*Dpyd*) was induced in hepatocytes but repressed in all
 675 other cell types (<https://doi.org/10.6084/m9.figshare.12728522>).

676 The number of DEGs in hepatocytes correlated with
 677 basal *Ahr* expression levels in control samples. Central and
 678 midcentral hepatocytes exhibited the highest basal *Ahr*
 679 expression levels (detected in 79% and 65% of nuclei,
 680 respectively) (Figure 3B) and exhibited the most DEGs.
 681 Portal hepatocytes also exhibited a large number of DEGs
 682 (6346) despite a lower AhR expression level (detected in
 683 69%)

684 **Figure 3. (See previous page). TCDD-elicited differential gene expression in distinct hepatic cell subtypes.** (A) Cross-
 685 comparisons of DEGs (adjusted $P \leq .05$) between cell (sub)types. The number of DEGs (adjusted $P \leq .05$) determined for
 686 each nuclei cluster is provided in the diagonal boxes color-coded according to cell subtypes identified in Figure 1A. The
 687 number of common DEGs determined between each pair of cell types is provided in upper right portion of table in black font.
 688 The percentage of common DEGs between cell types is provided in the bottom left portion of table using 2 different colored
 689 fonts. The upper colored font represents the percent overlap of DEGs relative to the cell subtype for the column, while the
 690 lower colored font represents the percent overlap of DEGs relative to the cell subtype for the row. An example of percent
 691 calculations is shown between B cells and T cells using arrows (eg, 301/552 = 0.545). (B) UMAP visualization of *Ahr* expression
 692 in all nuclei from vehicle control samples. (C) Comparison of pseudobulk and bulk RNA-seq analyses for up- and down-
 693 regulated genes detected in both datasets.

2020

Hepatotoxicant Single-Nuclei RNA Sequencing 7

707 only 17% of portal nuclei) suggesting secondary or tertiary
 708 factors (eg, chromatin accessibility, metabolite gradient,
 709 cell-cell interactions) contributed to TCDD responsiveness.
 710 Induction of classic AhR target genes was not detected in all
 711 cell types (<https://doi.org/10.6084/m9.figshare.12728522>)
 712 and exhibited fold-change differences between cell types.
 713 For instance, *Cyp1a1* was induced 2736-fold in portal
 714 hepatocytes, consistent with reports in bulk RNA-seq
 715 analyses. The 1177-fold repression of *Ces3b* reported in
 716 bulk RNA-seq was comparable to 3089-fold repression
 717 observed in central hepatocytes. Many genes went from
 718 undetected to detected, confounding fold-change estimates
 719 (ie, division by zero), though these genes were typically
 720 significantly induced in bulk RNA-seq. For example, *Gpnmb*
 721 was induced 1206-fold in our bulk RNA-seq dataset but only
 722 detected in macrophage following TCDD treatment in the
 723 snSeq dataset. A large number of zeroes is expected in
 724 scSeq/snSeq resulting from either absent expression or
 725 dropouts.

726 To compare single-nuclei with bulk RNA-seq data, snSeq
 727 data were first converted to “pseudo-bulk” data by summing
 728 read counts across all nuclei to approximate bulk expres-
 729 sion. Differential gene expression analysis for our pseudo-
 730 bulk data identified 2812 DEGs (adjusted $P \leq .05$ and
 731 $|fold change| \geq 2$), 2544 of which were also detected in bulk
 732 RNA-seq, with 1005 induced and 550 repressed in both
 733 analyses (Figure 3C). Only 27 genes showed divergent
 734 expression (eg, induced in one dataset and repressed in the
 735 other). Owing to the substantial technological differences in
 736 determining transcript counts, some differences are ex-
 737 pected. In addition, some genes may differ due to diurnal
 738 rhythm (eg, *Alas1*) or cell type biases (eg, macrophage genes
 739 *Adgre4* and *Clec4f*).
 740

741 **TCDD Elicits Unique Functional Changes in Cell 742 Populations**

743 To identify enriched cellular pathways, processes, and
 744 functions associated within specific cell (sub)types, all
 745 ^{Q7} constitutively expressed genes and DEGs were analyzed in
 746 control and treated samples. Enrichment scores were
 747 calculated for 6513 gene sets obtained from the Gene Set
 748 Knowledgebase (GSKB) for each nucleus independent of cell
 749 type classification. UMAP visualization of functional
 750 enrichment highlights TCDD-elicited shifts in enriched
 751 functions within specific cell types, most notably hepato-
 752 cytes (<https://doi.org/10.6084/m9.figshare.12728528>).
 753 Pathways, processes, and functions enriched within specific
 754 cell (sub)types were consistent with their known physio-
 755 logical roles (Figure 4, inner ring). For instance, macro-
 756 phages were enriched in phagocytosis and inflammation
 757 gene sets while endothelial cells were enriched in vascula-
 758 ture related genes. Hepatocytes were largely enriched in
 759 genes associated with the metabolism of carbohydrates,
 760 lipids, amino acids, and bile acids, as well as 1 carbon
 761 metabolism, and were consistent with their expected zonal
 762 distribution. Specifically, amino acid metabolism and the
 763 coagulation cascade were enriched in the portal region,
 764 while lipid, bile acid, and phase I xenobiotic metabolism

765 were centrally enriched (Figure 4), as reported in a recent
 766 zonal proteomics study.³⁵
 767

768 We next examined nuclei for functional enrichment
 769 following TCDD treatment using enrichment score differ-
 770 ences (fold-change) between control and treated nuclei
 771 (Figure 4, outer ring). RAS signaling had the most highly
 772 connected node, suggesting high similarity in gene mem-
 773 bership with other nodes, particularly those associated with
 774 nonparenchymal cells. Metabolism pathways were largely
 775 associated with hepatocytes, including repression of
 776 cholesterol and triglyceride metabolism, and metabolism of
 777 selected amino acids, which were either induced or
 778 repressed (eg, Arg, Asp, Gln, Glu, Pro). Not surprisingly,
 779 xenobiotic metabolism was induced in all hepatocytes
 780 except central hepatocytes. This is due to the repression of
 781 several cytochrome P450s and high constitutive expression
 782 of phase I metabolism genes in central hepatocytes. Other
 783 notable gene sets with increased enrichment following
 784 treatment in hepatocytes included (1) “up-regulated in
 785 liver-specific HNF4α knockout,” suggesting TCDD repressed
 786 HNF4 signaling; and (2) “repressed in liver cancer,” sug-
 787 gesting transcriptomic inhibition consistent with the hep-
 788 atocarcinogenicity of TCDD.
 789

790 **Emergence of New Macrophage (Sub)types 791 Following Treatment**

792 A hallmark of TCDD exposure is the infiltration of im-
 793 mune cells into the liver.³³ Figures 1D and 2B show the
 794 increased presence of macrophages and neutrophils
 795 following treatment. Resident macrophages in a normal
 796 liver largely consist of KCs marked by high *Adgre1* (F4/80)
 797 expression. Upon injury, motile monocyte-derived macro-
 798 phages with high levels of *Itgam* (Cd11b) and *Ccr2* expres-
 799 sion, are recruited.¹⁷ Further analysis of macrophage nuclei
 800 identified 5 distinct clusters, of which 4 expressed high
 801 levels of *Adgre1* and *Cd5l* (Figure 5), while none exhibited
 802 high levels of *Itgam* (not detected) or *Ccr2* (expressed in
 803 ≤4% of control macrophages). Macrophage clusters 1, 2,
 804 and 3 not only expressed high levels of *Adgre1* and *Cd5l*, but
 805 also expressed high levels of *Gpnmb*, which was not present
 806 in KCs from control samples. Interestingly, comparable
 807 macrophage clusters were reported in a diet-induced NASH
 808 mouse model, described as NAMs, that also exhibited high
 809 *Trem2* expression.¹⁷ Although highly induced in our bulk
 810 RNA-seq dataset, we did not identify a single macrophage
 811 population among the 4 identified here expressing high
 812 *Trem2* levels, nor *Cd9*, as reported in NAMs by Xiong et al.¹⁶
 813 This is likely another example of a gene biased to the
 814 cytoplasm, as both genes are more abundant in the cytosol
 815 than nuclei in liver cells.³² However, segregating nuclei
 816 expressing *Gpnmb* does reveal significant enrichment in
 817 nuclei expressing *Trem2* and *Cd9* (<https://doi.org/10.6084/m9.figshare.12728588>). KC cluster 3 was also determined to
 818 express high levels of the cell cycle gene *Top2a*, possibly
 819 identifying a proliferating NAM subpopulation as these
 820 nuclei also abundantly expressed the NAM marker *Gpnmb*.
 821 The fourth and smallest cluster expressed high levels of
 822 *Bcl11a* and *Ccr9* (Figure 5B), and likely represent plasma-
 823 cytoid dendritic cells as previously reported.¹⁵
 824

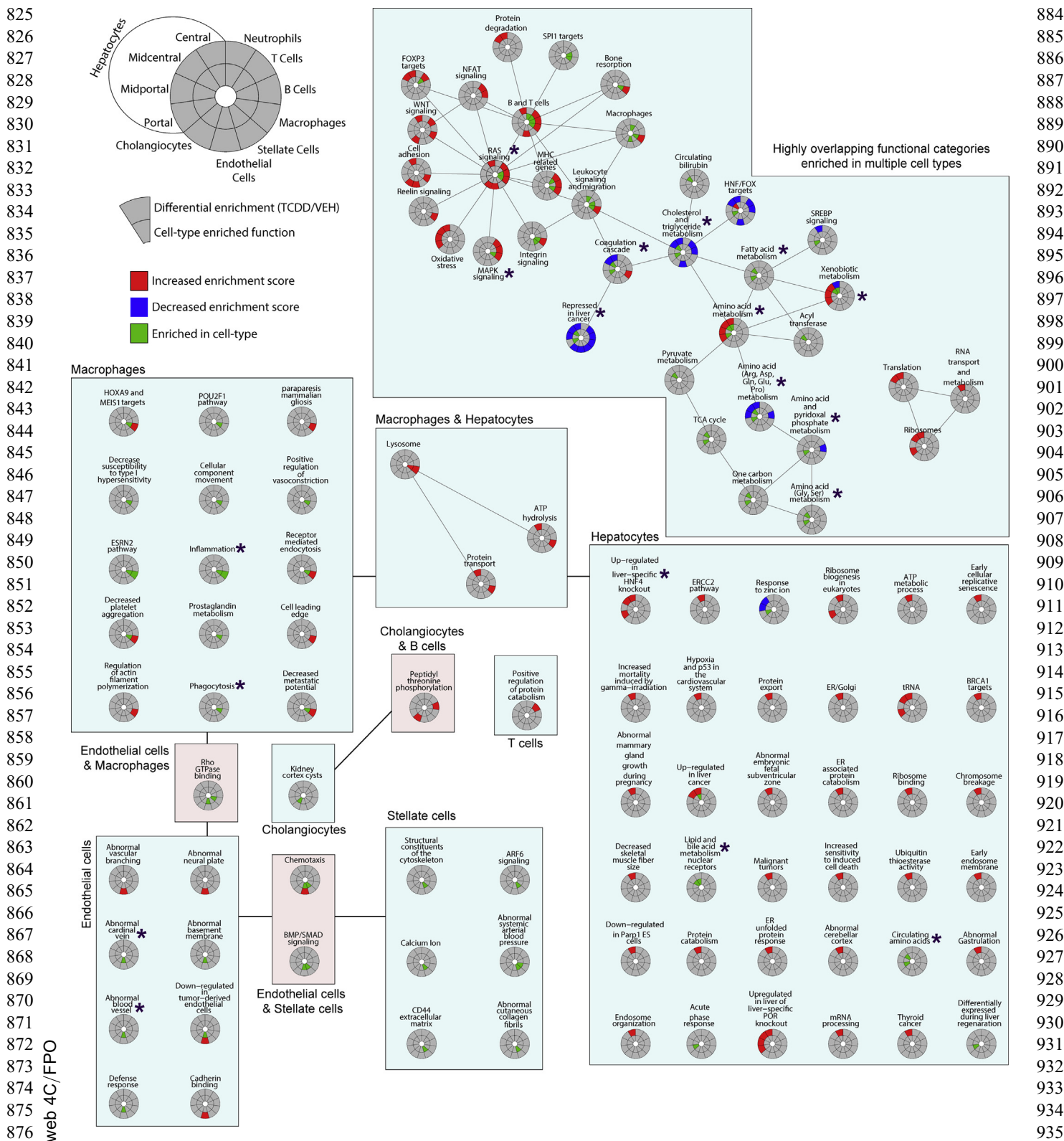


Figure 4. Gene set enrichment analysis of single-nuclei transcriptomes. Circos plots of functional enrichment analysis for each cell type indicates marker functions (adjusted $P \leq .05$ compared with other cell types; inner ring; green) and functions showing increased (red) or decreased (blue) enrichment scores following TCDD treatment (outer ring). Enrichment scores for 6513 gene sets were determined using Gene Set Variation Analysis, grouped based on gene membership similarity using Enrichment Map, and summarized using AutoAnnotate, followed by manual curation, as described in the Materials and Methods. Asterisks indicate functions discussed in the manuscript.

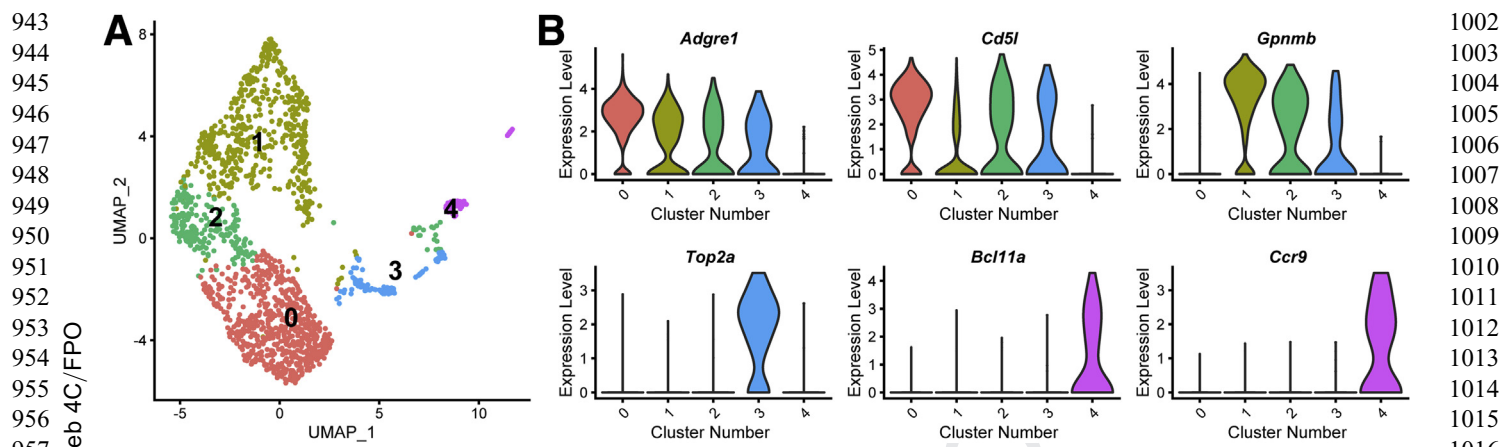


Figure 5. Clustering of macrophage nuclei transcriptomes. (A) UMAP plot of macrophage nuclei determined at 0.2 resolution using Seurat. (B) Violin plots of the expression levels of unique genes that distinguish macrophage subtypes.

Discussion

Single-cell/nuclei transcriptomics not only has provided novel insight into molecular mechanisms involved in cellular development and normal cell function, but has also identified and characterized rare cell (sub)types.^{13–17,36} It has the potential to further elucidate the mechanisms of toxicity elicited by exogenous agents that disrupt normal cellular functions. Most importantly, it enables the assessment of cell type-specific responses, thus integrating systemic (multiorgan) and local events within the context of a tissue or organ. In this study, we used a nuclei-based strategy to minimize potential biases in cell (sub)types due to toxicity that was also logistically feasible within a large dose-response and time-course study. Similar strategies have been used for neurons which vary wildly in shape, density, and other cellular characteristics, as well as post-mortem human tissues with good success.^{37,38}

Single-cell analyses have been performed on mouse and human liver samples, though most involved enrichment for either hepatocytes or nonparenchymal cells (NPCs).^{15–17,39} Using a single-nuclei approach, we captured the expected hepatic cell types identified in previous studies with hepatocyte nuclei highly represented, given that they compose ≥80% of the liver cell population. Consequently, immune cells such as the plasmacytoid dendritic cells and capsule macrophages identified in NPC-enriched samples, were difficult to identify, particularly in control samples.¹⁵ A potential solution to counter this unequal hepatocyte sampling bias could be fluorescence-activated cell sorting separation of nuclei based on DNA, as NPCs are enriched in the diploid (2N) population while hepatocyte nuclei are often polyploid.⁴⁰ However, TCDD altered liver cell ploidy (<https://doi.org/10.6084/m9.figshare.12728540>),⁴¹ which may bias the relative proportions of distinct cell types, and therefore we did not separate nuclei by ploidy in this study. While our snSeq dataset could not estimate the total number of each cell type, the emergence of new cell populations and the transcriptomic changes of resident cells could be distinguished. Distinguishing the loss of cell (sub)types due to toxicity from de/trans-differentiation represents a unique challenge.

Our single-nuclei strategy highlighted several advantages over single-cell analysis to assess hepatotoxins. First, nuclei isolated from frozen samples could clearly be classified as distinct known hepatic cell types. Second, despite higher representation of nuclear-biased genes, TCDD-elicited differential expression determined by bulk RNA-seq was largely recapitulated in a pseudo-bulk version of our snSeq dataset, with only 38 genes showing contrary results, which could be due to other confounding factors (eg, different technologies, diurnal rhythm). However, our dataset was enriched with nuclear-biased genes while other cell type markers, such as the cholangiocyte marker *Sox9*, were not detected. Single-nuclei droplets may also be more susceptible to ambient RNA contamination, though our mitochondrial gene expression content was low. Despite differences in messenger RNA (mRNA) capture, sequencing, counting, and analysis, the strong correspondence indicates that snSeq is a viable alternative, with distinct advantages over scSeq analysis.

Hepatotoxins can elicit zonal toxicity based on their mode of action and the functional gradient of the lobule chords (central vein to portal vein). Toxicants not requiring bioactivation commonly damage periportal regions when first encountered via the portal vein. Conversely, toxicants requiring bioactivation are more often toxic to pericentral regions due to higher basal expression of phase I metabolism enzymes (eg, cytochrome P450s). TCDD is a periportal hepatotoxicant, though damage spans the periportal to pericentral regions (panacinar) with increasing dose. Interestingly, pericentral hepatocytes were most responsive to TCDD, followed by periportal hepatocytes. TCDD primarily accumulates in central hepatocytes due to the induction of CYP1A2, a phase I metabolism enzyme that sequesters TCDD.²⁰ The high dose of TCDD that caused panacinar damage together with the higher basal expression of *Ahr* in central hepatocytes likely coalesced to elicit the large number of DEGs in this region. TCDD also reduced the portal hepatocyte representation. Emerging spatial transcriptomics technologies are expected to provide further insights into the apparent decrease in periportal cells, as well as other cell-specific changes.

1002
1003
1004
1005
1006
1007
1008
1009
1010
1011
1012
1013
1014
1015
1016
1017
1018
1019
1020
1021
1022
1023
1024
1025
1026
1027
1028
1029
1030
1031
1032
1033
1034
1035
1036
1037
1038
1039
1040
1041
1042
1043
1044
1045
1046
1047
1048
1049
1050
1051
1052
1053
1054
1055
1056
1057
1058
1059
1060

Ultimately, snSeq provided novel insight into cell-specific gene expression and the roles of distinct cell populations. RAS/MAPK signaling was activated in hepatic NPCs in response to TCDD. Previous studies have linked RAS/MAPK signaling to inflammation in human NAFLD, likely through the production of growth factors, cytokines, chemokines, and adhesion molecules.⁴² Moreover, TCDD repressed hepatocyte proliferation,⁴³ and RAS induction by TCDD in HepG2 cells does not activate the downstream effector, MAPK.⁴⁴ The lack of hepatocyte enrichment is also consistent with the inhibition of hepatocyte proliferation and infiltration of immune cells. Further investigation of macrophage subpopulations identified a high *Gpnmb*-expressing KC population following TCDD treatment, which was also reported in a diet-induced NASH model¹⁷ and in humans with steatosis or NASH,⁴⁵ suggesting conserved molecular events across disparate etiologies and species. In agreement with the loss of liver-specific gene expression,⁴⁶ we find enriched genes that were also upregulated in a liver-specific HNF4 knockout model, a transcription factor essential for liver-specific gene expression.⁴⁷ Similarly, there was decreased expression of genes repressed in liver cancer, consistent with TCDD being a known mouse liver carcinogen. Decreased enrichment was observed in most cell types, as the gene set was produced from whole-tissue expression profiling, highlighting some caveats when examining functional changes using single-cell/nuclei data.

In conclusion, snSeq represents a valuable strategy to characterize cell-specific responses of hepatotoxins. Despite known biases in nuclear and cytosolic transcript levels, single-nuclei transcriptomic data accurately characterize the differential expression elicited by TCDD as reflected in (1) the consistency with bulk gene expression data, (2) the identification of NASH associated macrophages, and (3) changes in functional enrichment of pathways associated with TCDD-elicited hepatotoxicity. Furthermore, the analysis of frozen samples enables comprehensive dose- and time-dependent investigation of cell-specific adverse effects.

Materials and Methods

Animals and Treatment

Male C57BL/6 mice aged postnatal day (PND) 25 from Charles River Laboratories (Portage, MI) were housed in Innocages (Innovive, San Diego, CA) with ALPHA-dri bedding (Shepherd Specialty Papers, Chicago, IL) at 30%-40% humidity and a 12-hour light/dark cycle. Animals were fed ad libitum Harlan Teklad 22/5 Rodent Diet 8940 (Harlan Teklad, Madison, WI), with free access to Aquavive water (Innovive, San Diego, CA). PND 28 mice were orally gavaged with sesame oil vehicle (Sigma-Aldrich, St Louis, MO) or 30 µg/kg TCDD (AccuStandard, New Haven, CT) every 4 days for 28 days (7 treatments total). On day 28 (PND 52), animals were euthanized by CO₂ asphyxiation, and livers were immediately collected, frozen in liquid nitrogen, and stored at -80°C. All procedures were approved by the Michigan State University Institutional Animal Care and Use Committee.

Nuclei Isolation

Nuclei were isolated from frozen liver samples (~200 mg) as previously described (<https://doi.org/10.17504/protocols.io.3fgjkw>). Briefly, livers were diced in EZ Lysis Buffer (Sigma-Aldrich), homogenized using a disposable dounce homogenizer, and incubated on ice for 5 minutes. The homogenate was filtered using a 70-µm cell strainer, transferred to microcentrifuge tube, and centrifuged at 500 g and 4°C for 5 minutes. The supernatant was removed, and fresh EZ lysis buffer was added for an additional 5 minutes on ice following by centrifugation at 500 g and 4°C for 5 minutes. The nuclei pellet was washed twice in nuclei wash and resuspend buffer (1× phosphate-buffered saline, 1% bovine serum albumin, 0.2-U/µL RNase inhibitor) with 5-minute incubations on ice. Following the washes, the nuclei pellet was resuspended in nuclei wash and resuspend buffer containing DAPI (10 µg/mL). The resuspended nuclei were filtered with 40-µm strainer and immediately underwent fluorescence-activated cell sorting using a BD FACSAria IIU (BD Biosciences, San Jose, CA) with 70-µm nozzle at the MSU Pharmacology and Toxicology Flow Cytometry Core (druggdiscovery.msu.edu/facilities/flow-cytometry-core; <https://doi.org/10.6084/m9.figshare.12728540>). Sorted nuclei were immediately processed for snSeq.

snSeq and Data Analysis

Libraries were prepared using the 10x Genomics Chromium Single Cell 3' v3 kit and submitted for 150-bp paired-end sequencing at a depth ≥50,000 reads/cell using the HiSeq 4000 at Novogene (Beijing, China). Raw sequencing data were deposited in the Gene Expression Omnibus (GEO) (GSE148339). Following sequencing quality control, Cell-Ranger v3.0.2 (10x Genomics) was used to align reads to a custom reference genome (mouse mm10 release 93 genome build) which included introns and exons to consider pre-mRNA and mature mRNA present in the nuclei.

Raw counts were further analysed using Seurat v3.1.1.⁴⁸ Each sample was filtered for (1) genes expressed in at least 3 nuclei, (2) nuclei that express at least 100 genes, and (3) ≤1% mitochondrial genes. Additional quality control was performed using the scater package (v1.10.1). The DoubtFinder v2.0.2 package excluded putative doublets from subsequent analyses. Clustering of nuclei was performed using Seurat integration tools at a resolution of 0.2 and annotated using a semiautomated strategy by comparison to 3 published datasets (isolated hepatocytes sequenced by massively parallel scSeq [MARS-seq; GSE84498]; isolated hepatic NPCs by MARS-Seq [GSE108561]; isolated NPCs using the 10x Genomics platform [GSE129516]). Marker genes for individual nuclei clusters were also manually examined to verify annotation. Trajectory inference of hepatocytes was performed using Slingshot.³⁴

Gene Set Enrichment Analysis

Gene set enrichment analysis was performed on transcriptomes of individual nuclei using the Gene Set Variation Analysis (GSVA v1.30.0) package⁴⁹ with a minimum of 10 genes and maximum of 300 gene per gene set. Mouse gene

2020

Hepatotoxicant Single-Nuclei RNA Sequencing 11

sets were obtained from the GSKB (ge-lab.org/gskb/) filtered to only include MSIGDB, GENESIGDB, SMPDB, GO, KEGG, REACTOME, EHMN, MIRNA, MICROCOsm, MIRTARBASE, MPO, PID, PANTHER, BIOCARTA, INOH, NETPATH, WIKIPATHWAYS, MOUSECYC, TF, and TFACTS gene sets (6513 total). Human-based (eg, HPO), exposure-based (eg, DRUGBANK), or gene sets with limited annotation (eg, LIT) were excluded. Uniform Manifold Approximation and Projection (UMAP) reduction using the first 30 principal components analysis dimensions was used for visualization using original cell type annotations. For the visualization of marker and differentially enriched pathways, a network of gene sets was generated using the Enrichment Map plugin for Cytoscape.⁵⁰ Nodes were summarized using Auto-Annotate⁵¹ and subsequently manually curated. Nodes were redrawn using the Enhanced Graphics package.

Data and Code Availability

Raw and processed single-nuclei sequencing data is deposited in the GEO (<https://www.ncbi.nlm.nih.gov/geo/>) with the accession ID GSE148339. The final Seurat object including clustering, prediction scores, and annotation can be downloaded from the GEO repository or a compressed version from Dataverse (<https://doi.org/10.7910/DVN/WGFSNO>). Publically available datasets used to compare annotation were obtained from GEO under accession IDs GSE84498 GSE108561, and GSE129516. Bulk RNA-seq data for comparison with pseudobulk analysis was also obtained from GEO under accession ID GSE87543. Gene sets for gene set enrichment analysis were downloaded from the GSKB (ge-lab.org/gskb/). Analysis code for the processing and analysis of snSeq data can be obtained at <https://zacharewskilab.github.io/snseq-2doses-analysis/>. All authors had access to the study data and reviewed and approved the final manuscript.

References

- Gu X, Manautou JE. Molecular mechanisms underlying chemical liver injury. *Expert Rev Mol Med* 2012;14:e4.
- Hornberg JJ, Laursen M, Brenden N, Persson M, Thøgaard AV, Toft DB, Mow T. Exploratory toxicology as an integrated part of drug discovery. Part I: why and how. *Drug Discov today* 2014;19:1131–1136.
- Yorita Christensen KL, Carrico CK, Sanyal AJ, Gennings C. Multiple classes of environmental chemicals are associated with liver disease: NHANES 2003-2004. *Int J Hyg Environ Health* 2013;216:703–709.
- Cave M, Appana S, Patel M, Falkner KC, McClain CJ, Brock G. Polychlorinated biphenyls, lead, and mercury are associated with liver disease in American adults: NHANES 2003-2004. *Environ Health Perspect* 2010; 118:1735–1742.
- Heindel JJ, Blumberg B, Cave M, Machtlinger R, Mantovani A, Mendez MA, Nadal A, Palanza P, Panzica G, Sargis R, Vandenberg LN, Vom Saal F. Metabolism disrupting chemicals and metabolic disorders. *Reprod Toxicol* 2017;68:3–33.

- Fader KA, Nault R, Kirby MP, Markous G, Matthews J, Zacharewski TR. Convergence of hepcidin deficiency, systemic iron overloading, heme accumulation, and REV-ERBalpha/beta activation in aryl hydrocarbon receptor-elicited hepatotoxicity. *Toxicol Appl Pharmacol* 2017;321:1–17.
- Nault R, Fader KA, Ammendolia DA, Dornbos P, Potter D, Sharratt B, Kumagai K, Harkema JR, Lunt SY, Matthews J, Zacharewski T. Dose-dependent metabolic reprogramming and differential gene expression in TCDD-elicited hepatic fibrosis. *Toxicol Sci* 2016; 154:253–266.
- Pierre S, Chevallier A, Teixeira-Clerc F, Ambolet-Camoit A, Bui LC, Bats AS, Fournet JC, Fernandez-Salguero P, Aggerbeck M, Lotersztajn S, Barouki R, Coumoul X. Aryl hydrocarbon receptor-dependent induction of liver fibrosis by dioxin. *Toxicol Sci* 2014; 137:114–124.
- Taylor KW, Novak RF, Anderson HA, Birnbaum LS, Blystone C, Devito M, Jacobs D, Kohrle J, Lee DH, Rylander L, Rignell-Hydbom A, Tornero-Velez R, Turyk ME, Boyles AL, Thayer KA, Lind L. Evaluation of the association between persistent organic pollutants (POPs) and diabetes in epidemiological studies: a national toxicology program workshop review. *Environ Health Perspect* 2013;121:774–783.
- Henriksen GL, Ketchum NS, Michalek JE, Swaby JA. Serum dioxin and diabetes mellitus in veterans of Operation Ranch Hand. *Epidemiology* 1997;8:252–258.
- Hart SN, Li Y, Nakamoto K, Subileau EA, Steen D, Zhong XB. A comparison of whole genome gene expression profiles of HepaRG cells and HepG2 cells to primary human hepatocytes and human liver tissues. *Drug Metab Dispos* 2010;38:988–994.
- Browaeys R, Saelens W, Saeys Y. NicheNet: modeling intercellular communication by linking ligands to target genes. *Nat Methods* 2020;17:159–162.
- Su X, Shi Y, Zou X, Lu ZN, Xie G, Yang JYH, Wu CC, Cui XF, He KY, Luo Q, Qu YL, Wang N, Wang L, Han ZG. Single-cell RNA-Seq analysis reveals dynamic trajectories during mouse liver development. *BMC Genomics* 2017;18:946.
- Habib N, Li Y, Heidenreich M, Swiech L, Avraham-David I, Trombetta JJ, Hession C, Zhang F, Regev A. Div-Seq: Single-nucleus RNA-Seq reveals dynamics of rare adult newborn neurons. *Science* 2016;353:925–928.
- Bahar Halpern K, Shenhav R, Massalha H, Toth B, Egozi A, Massasa EE, Medgalia C, David E, Giladi A, Moor AE, Porat Z, Amit I, Itzkovitz S. Paired-cell sequencing enables spatial gene expression mapping of liver endothelial cells. *Nat Biotechnol* 2018;36:962–970.
- Bahar Halpern K, Shenhav R, Matcovitch-Natan O, Toth B, Lemze D, Golan M, Massasa EE, Baydatch S, Landen S, Moor AE, Brandis A, Giladi A, Avihail AS, David E, Amit I, Itzkovitz S. Single-cell spatial reconstruction reveals global division of labour in the mammalian liver. *Nature* 2017;542:352–356.
- Xiong X, Kuang H, Ansari S, Liu T, Gong J, Wang S, Zhao XY, Ji Y, Li C, Guo L, Zhou L, Chen Z, Leon-Mimila P, Chung MT, Kurabayashi K, Opp J,

- 1297 Campos-Perez F, Villamil-Ramirez H, Canizales-
1298 Quinteros S, Lyons R, Lumeng CN, Zhou B, Qi L, Huer-
1299 tas-Vazquez A, Lusis AJ, Xu XZS, Li S, Yu Y, Li JZ,
1300 Lin JD. Landscape of intercellular crosstalk in healthy
1301 and NASH liver revealed by single-cell secretome gene
1302 analysis. *Mol Cell* 2019;75:644–660.e5. 1356
1303 1357
- 1303 Anundi I, Lahteenmaki T, Rundgren M, Moldeus P,
1304 Lindros KO. Zonation of acetaminophen metabolism and
1305 cytochrome P450 2E1-mediated toxicity studied in iso-
1306 lated periportal and perivenous hepatocytes. *Biochem
1307 Pharmacol* 1993;45:1251–1259.
- 1308 Boverhof DR, Burgoon LD, Tashiro C, Sharratt B,
1309 Chittim B, Harkema JR, Mendrick DL, Zacharewski TR.
1310 Comparative toxicogenomic analysis of the hepatotoxic
1311 effects of TCDD in Sprague Dawley rats and C57BL/6
1312 mice. *Toxicol Sci* 2006;94:398–416.
- 1313 Santostefano MJ, Richardson VM, Walker NJ, Blanton J,
1314 Lindros KO, Lucier GW, Alcasey SK, Birnbaum LS. Dose-
1315 dependent localization of TCDD in isolated centrilobular
1316 and periportal hepatocytes. *Toxicol Sci* 1999;52:9–19.
- 1317 Fader KA, Nault R, Doskey CM, Fling RR,
1318 Zacharewski TR. 2,3,7,8-Tetrachlorodibenzo-p-dioxin
1319 abolishes circadian regulation of hepatic metabolic ac-
1320 tivity in mice. *Sci Rep* 2019;9:6514.
- 1321 Lake BB, Chen S, Sos BC, Fan J, Kaeser GE, Yung YC,
1322 Duong TE, Gao D, Chun J, Kharchenko PV, Zhang K.
1323 Integrative single-cell analysis of transcriptional and
1324 epigenetic states in the human adult brain. *Nat Bio-
1325 technol* 2018;36:70–80.
- 1326 Zeng W, Jiang S, Kong X, El-Ali N, Ball AR Jr, Ma CI,
1327 Hashimoto N, Yokomori K, Mortazavi A. Single-nucleus
1328 RNA-seq of differentiating human myoblasts reveals the
1329 extent of fate heterogeneity. *Nucleic Acids Res* 2016;
1330 44:e158.
- 1331 Habib N, Avraham-David I, Basu A, Burks T, Shekhar K,
1332 Hofree M, Choudhury SR, Aguet F, Gelfand E, Ardlie K,
1333 Weitz DA, Rozenblatt-Rosen O, Zhang F, Regev A.
1334 Massively parallel single-nucleus RNA-seq with DroNc-
1335 seq. *Nat Methods* 2017;14:955–958.
- 1336 Nault R, Fader KA, Zacharewski T. RNA-Seq versus
1337 oligonucleotide array assessment of dose-dependent
1338 TCDD-elicted hepatic gene expression in mice. *BMC
1339 Genomics* 2015;16:373.
- 1340 Alvarez M, Rahmani E, Jew B, Garske KM, Miao Z,
1341 Benhammou JN, Ye CJ, Pisegna JR, Pietiläinen KH,
1342 Halperin E, Pajukanta P. Enhancing droplet-based sin-
1343 gle-nucleus RNA-seq resolution using the semi-
1344 supervised machine learning classifier DIEM. *Sci Rep*
1345 2020;10:11019.
- 1346 Franzén O, Gan L-M, Björkegren JLM. PanglaoDB: a web
1347 server for exploration of mouse and human single-cell
1348 RNA sequencing data. *Database (Oxford)* 2019;
1349 2019:baz046.
- 1350 Nonaka H, Tanaka M, Suzuki K, Miyajima A. Develop-
1351 ment of murine hepatic sinusoidal endothelial cells
1352 characterized by the expression of hyaluronan receptors.
1353 *Dev Dyn* 2007;236:2258–2267.
- 1354 Masyuk TV, Huang BQ, Ward CJ, Masyuk AI, Yuan D,
1355 Splinter PL, Punyashthiti R, Ritman EL, Torres VE,
Harris PC, LaRusso NF. Defects in cholangiocyte
fibrocystin expression and ciliary structure in the PCK
rat. *Gastroenterology* 2003;125:1303–1310. 1356
1357
- 1358 Zhang Z, Cotta CV, Stephan RP, deGuzman CG,
1359 Klug CA. Enforced expression of EBF in hematopoietic
1360 stem cells restricts lymphopoiesis to the B cell lineage.
1361 *EMBO J* 2003;22:4759–4769.
- 1362 Smith X, Taylor A, Rudd CE. T-cell immune adaptor
1363 SKAP1 regulates the induction of collagen-induced
1364 arthritis in mice. *Immunol Lett* 2016;176:122–127.
- 1365 Bahar Halpern K, Caspi I, Lemze D, Levy M, Landen S,
1366 Elinav E, Ulitsky I, Itzkovitz S. Nuclear retention of mRNA
1367 in mammalian tissues. *Cell Rep* 2015;13:2653–2662.
- 1368 Fader KA, Nault R, Zhang C, Kumagai K, Harkema JR,
1369 Zacharewski TR. 2,3,7,8-Tetrachlorodibenzo-p-dioxin
1370 (TCDD)-elicited effects on bile acid homeostasis: Alter-
1371 ations in biosynthesis, enterohepatic circulation, and
1372 microbial metabolism. *Sci Rep* 2017;7:5921.
- 1373 Street K, Risso D, Fletcher RB, Das D, Ngai J, Yosef N,
1374 Purdom E, Dudoit S. Slingshot: cell lineage and pseu-
1375 dotime inference for single-cell transcriptomics. *BMC
1376 Genomics* 2018;19:477.
- 1377 Ben-Moshe S, Shapira Y, Moor AE, Manco R, Veg T,
1378 Bahar Halpern K, Itzkovitz S. Spatial sorting enables
1379 comprehensive characterization of liver zonation. *Nat
1380 Metab* 2019;1:899–911.
- 1381 Iacono G, Massoni-Badosa R, Heyn H. Single-cell tran-
1382 scriptomics unveils gene regulatory network plasticity.
1383 *Genome Biol* 2019;20:110.
- 1384 Bakken TE, Hodge RD, Miller JA, Yao Z, Nguyen TN,
1385 Aevermann B, Barkan E, Bertagnoli D, Casper T, Dee N,
1386 Garren E, Goldy J, Graybuck LT, Kroll M, Lasken RS,
1387 Lathia K, Parry S, Rimorin C, Scheuermann RH,
1388 Schork NJ, Shehata SI, Tieu M, Phillips JW, Bernard A,
1389 Smith KA, Zeng H, Lein ES, Tasic B. Single-nucleus and
1390 single-cell transcriptomes compared in matched cortical
1391 cell types. *PLoS One* 2018;13:e0209648.
- 1392 Krishnaswami SR, Grindberg RV, Novotny M,
1393 Venepally P, Lacar B, Bhutani K, Linker SB, Pham S,
1394 Erwin JA, Miller JA, Hodge R, McCarthy JK, Kelder M,
1395 McCorrison J, Aevermann BD, Fuertes FD,
1396 Scheuermann RH, Lee J, Lein ES, Schork N,
1397 McConnell MJ, Gage FH, Lasken RS. Using single nuclei
1398 for RNA-seq to capture the transcriptome of postmortem
1399 neurons. *Nat Protoc* 2016;11:499–524.
- 1400 MacParland SA, Liu JC, Ma XZ, Innes BT, Bartczak AM,
1401 Gage BK, Manuel J, Khuu N, Echeverri J, Linares I,
1402 Gupta R, Cheng ML, Liu LY, Camat D, Chung SW,
1403 Seliga RK, Shao Z, Lee E, Ogawa S, Ogawa M,
1404 Wilson MD, Fish JE, Selzner M, Ghanekar A, Grant D,
1405 Greig P, Sapisochin G, Selzner N, Winegarden N,
1406 Adeyi O, Keller G, Bader GD, McGilvray ID. Single cell
1407 RNA sequencing of human liver reveals distinct intra-
1408 hepatic macrophage populations. *Nat Commun* 2018;
1409 9:4383.
- 1410 Digernes V, Bolund L. The ploidy classes of adult mouse
1411 liver cells. A methodological study with flow cytometry
1412 and cell sorting. *Virchows Arch B Cell Pathol Incl Mol
1413 Pathol* 1979;32:1–10.
- 1414 Moreno-Marin N, Merino JM, Alvarez-Barrientos A,
Patel DP, Takahashi S, Gonzalez-Sancho JM,

- 1415 Gandolfo P, Rios RM, Munoz A, Gonzalez FJ, Fernandez-Salguero PM. Aryl hydrocarbon receptor promotes liver polyploidization and inhibits PI3K, ERK, and Wnt/beta-catenin signaling. *iScience* 2018;4:44–63.
- 1416 42. Jimenez-Castro MB, Cornide-Petronio ME, Gracia-Sancho J, Casillas-Ramirez A, Peralta C. Mitogen activated protein kinases in steatotic and non-steatotic livers submitted to ischemia-reperfusion. *Int J Mol Sci* 2019; 20:1785.
- 1417 43. Jackson DP, Li H, Mitchell KA, Joshi AD, Elferink CJ. Ah receptor-mediated suppression of liver regeneration through NC-XRE-driven p21Cip1 expression. *Mol Pharmacol* 2014;85:533–541.
- 1418 44. Yamaguchi M, Hankinson O. 2,3,7,8-Tetrachlorodibenzopdioxin suppresses the growth of human liver cancer HepG2 cells in vitro: Involvement of cell signaling factors. *Int J Oncol* 2018;53:1657–1666.
- 1419 45. Katayama A, Nakatsuka A, Eguchi J, Murakami K, Teshigawara S, Kanzaki M, Nunoue T, Hida K, Wada N, Yasunaka T, Ikeda F, Takaki A, Yamamoto K, Kiyonari H, Makino H, Wada J. Beneficial impact of Gpnmb and its significance as a biomarker in nonalcoholic steatohepatitis. *Sci Rep* 2015;5:16920.
- 1420 46. Nault R, Fader KA, Harkema JR, Zacharewski T. Loss of liver-specific and sexually dimorphic gene expression by aryl hydrocarbon receptor activation in C57BL/6 mice. *PLoS One* 2017;12:e0184842.
- 1421 47. Ohguchi H, Tanaka T, Uchida A, Magoori K, Kudo H, Kim I, Daigo K, Sakakibara I, Okamura M, Harigae H, Sasaki T, Osborne TF, Gonzalez FJ, Hamakubo T, Kodama T, Sakai J. Hepatocyte nuclear factor 4alpha contributes to thyroid hormone homeostasis by cooperatively regulating the type 1 iodothyronine deiodinase gene with GATA4 and Kruppel-like transcription factor 9. *Mol Cell Biol* 2008;28:3917–3931.
- 1422 48. Butler A, Hoffman P, Smibert P, Papalexi E, Satija R. Integrating single-cell transcriptomic data across different conditions, technologies, and species. *Nat Biotechnol* 2018;36:411–420.
- 1423 49. Hanzelmann S, Castelo R, Guinney J. GSVA: gene set variation analysis for microarray and RNA-seq data. *BMC bioinformatics* 2013;14:7.
- 1424 50. Merico D, Isserlin R, Stueker O, Emili A, Bader GD. Enrichment map: a network-based method for gene-set enrichment visualization and interpretation. *PLoS One* 2010;5:e13984.
- 1425 51. Kucera M, Isserlin R, Arkhangorodsky A, Bader GD. AutoAnnotate: a Cytoscape app for summarizing networks with semantic annotations. *F1000Res* 2016; 5:1717.
-
- Received April 28, 2020. Accepted July 31, 2020.
- Correspondence**
Address correspondence to: Tim Zacharewski, PhD, Michigan State University, 1129 Farm Lane, Room 248, East Lansing, MI 48824. e-mail: tzachare@msu.edu; fax: ***.
- Acknowledgments**
The authors would like to thank Dr Luciano Martelotto (University of Melbourne) for his help in optimizing the nuclei isolation protocol for single-nuclei RNA sequencing, as well as the labs of Dr Jiande Lin (University of Michigan) and Dr Shalev Itzkovitz (Weizmann Institute of Science) for sharing processed datasets used to semi-automate cluster annotation.
- Conflicts of interest**
The authors disclose no conflicts.
- Funding**
This work was supported by the National Institute of Environmental Health Sciences Superfund Research Program (P42ES004911) (to Tim R. Zacharewski) and the National Human Genome Research Institute (R21HG010789) to Tim R. Zacharewski and Sudin Bhattacharya. Tim R. Zacharewski and Sudin Bhattacharya are partially supported by AgBioResearch at Michigan State University.